Research Article

A Consistent Immersed Finite Element Method for the Interface Elasticity Problems

Sangwon Jin, Do Y. Kwak, and Daehyeon Kyeong

Korea Advanced Institute of Science and Technology, Daejeon 305-701, Republic of Korea

Correspondence should be addressed to Do Y. Kwak; kdy@kaist.ac.kr

We propose a new scheme for elasticity problems having discontinuity in the coefficients. In the previous work (Kwak et al., 2014), the authors suggested a method for solving such problems by finite element method using nonfitted grids. The proposed method is based on the P_1-nonconforming finite element methods with stabilizing terms. In this work, we modify the method by adding the consistency terms, so that the estimates of consistency terms are not necessary. We show optimal error estimates in H^1 and divergence norms under minimal assumptions. Various numerical experiments also show optimal rates of convergence.

1. Introduction

Linear elasticity equations are important governing equations in continuum mechanics, they describe how solid objects are deformed when external forces are applied on them. In particular, elasticity interface problems are important in various fields such as solid mechanics, material sciences, and biological sciences. There are various numerical methods to solve these problems such as finite difference methods, finite volume methods, and finite element methods; see [1–6] and references therein. But the problems involving composite materials lead to the discontinuity in the coefficients of the governing equations. In this case, there are two types of numerical methods from the point of view of mesh generation. In the first type, people solve the problems by using fitted grid which is created to align with the interface [7, 8]; another type is to use an unfitted (uniform) grid which is generated independently of the interface [9–15].

Fitted grid method is well known and the most widely used accurate method but it has weaknesses for the time dependent problems which include moving interface. In moving interface problems, we need to regenerate the appropriate mesh for the interface which changes according to time. Therefore, it is not adequate to apply to the moving interface problems since this mesh generation has considerable computational costs.

However, using a fixed grid has an obvious advantage that we can use the mesh in the previous time step, in the case when the interface changes over time. Therefore, it is suitable for moving interface problems. There are two classes of methods which belong to this type. One is the extended finite element method (XFEM) and the other is the immersed finite element method (IFEM). In the XFEM, they use enrichment basis functions in addition to the standard finite element basis. Therefore, they have more degrees of freedom than the standard FEM. In IFEM, the degrees of freedom are the same as the standard FEM basis; instead we modify the shape functions so as to satisfy the interface conditions along the interior interface. Recently, Lin et al. [9] have suggested a numerical method for solving elasticity problem with an interface using rotated Q_1-nonconforming finite element on uniform grids and Kwak et al. [10] proved the optimal error estimate for P_1-nonconforming finite element on triangular grids under an some extra regularity that the stress component belongs to H^2.

In this paper, we modify the numerical scheme studied in [10] for the elasticity problem with an interface. We add consistency terms in the bilinear form to avoid the consistency term estimate. As a result, the extra regularity assumption which is necessary to estimate the consistency term error in the previous work [10] can be avoided. We prove optimal error estimates by the standard framework of finite

element error analysis, which includes proving the coercivity and boundedness of the bilinear form.

The rest of our paper is organized as follows. In Section 2, we introduce a problem with interface along which Laplace-Young condition holds. In Section 3, we review the vector basis functions introduced in [10] based on the P_1 nonconforming elements satisfying the interface conditions and discretize the problem using (uniform) triangular grids. In Section 4, we prove the approximation property of our finite element space and the coercivity of our variational form. Next, we prove optimal H^1 and divergence norm error estimates. Finally, numerical experiments are presented in Section 5 for various Lamé constants and for shape interfaces.

2. Preliminaries

Let Ω be a connected, convex polygonal domain in $\mathbb{R}^2$ which is divided into two subdomains Ω^+ and Ω^- by C^2 interface $\Gamma = \partial\Omega^+ \cap \partial\Omega^-$; see Figure 1. We assume the subdomains Ω^+ and Ω^- are occupied by two different elastic materials. For a differentiable function $\mathbf{v} = (v_1, v_2)$ and a tensor $\boldsymbol{\tau} = \left(\begin{smallmatrix} \tau_{11} & \tau_{12} \\ \tau_{21} & \tau_{22} \end{smallmatrix}\right)$, we let

$$
\begin{aligned}
\nabla\mathbf{v} &= \begin{pmatrix} \dfrac{\partial v_1}{\partial x} & \dfrac{\partial v_1}{\partial y} \\ \dfrac{\partial v_2}{\partial x} & \dfrac{\partial v_2}{\partial y} \end{pmatrix}, \\
\operatorname{div}\boldsymbol{\tau} &= \begin{pmatrix} \dfrac{\partial \tau_{11}}{\partial x} + \dfrac{\partial \tau_{12}}{\partial y} \\ \dfrac{\partial \tau_{21}}{\partial x} + \dfrac{\partial \tau_{22}}{\partial y} \end{pmatrix}.
\end{aligned}
\tag{1}
$$

Then the displacement $\mathbf{u} = (u_1, u_2)$ of the elastic body under an external force satisfies the Navier-Lamé equation as follows:

$$-\operatorname{div}\boldsymbol{\sigma}(\mathbf{u}) = \mathbf{f} \quad \text{in } \Omega^s, \ (s = +, -), \tag{2}$$

$$[\mathbf{u}]_\Gamma = 0, \tag{3}$$

$$[\boldsymbol{\sigma}(\mathbf{u}) \cdot \mathbf{n}]_\Gamma = 0, \tag{4}$$

$$\mathbf{u} = 0 \quad \text{on } \partial\Omega, \tag{5}$$

where

$$
\begin{aligned}
\boldsymbol{\sigma}(\mathbf{u}) &= 2\mu\boldsymbol{\epsilon}(\mathbf{u}) + \lambda\operatorname{tr}(\boldsymbol{\epsilon}(\mathbf{u}))\,\boldsymbol{\delta}, \\
\boldsymbol{\epsilon}(\mathbf{u}) &= \frac{1}{2}\left(\nabla\mathbf{u} + \nabla\mathbf{u}^T\right)
\end{aligned}
\tag{6}
$$

are the stress tensor and the strain tensor, respectively, $\mathbf{n}$ is outward unit normal vector, $\boldsymbol{\delta}$ is the identity tensor, and $\mathbf{f} \in (L^2(\Omega))^2$ is the external force. Here

$$
\begin{aligned}
\lambda &= \frac{E\nu}{(1+\nu)(1-2\nu)}, \\
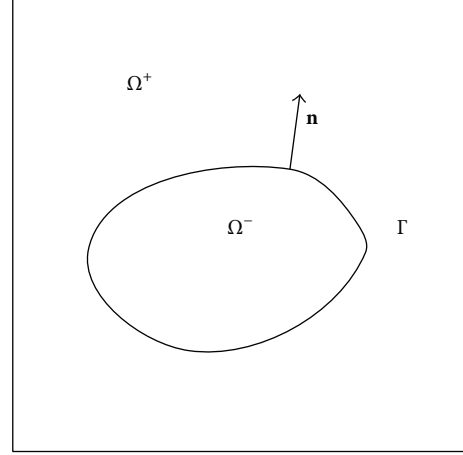\mu &= \frac{E}{2(1+\nu)}
\end{aligned}
\tag{7}
$$

FIGURE 1: A domain Ω with interface.

are the Lamé constants, satisfying $0 < \mu_1 < \mu < \mu_2$ and $0 < \lambda < \infty$, and E is Young's modulus and ν is the Poisson ratio. When the parameter $\lambda \to \infty$, this equation describes the behavior of nearly incompressible material. Since the material properties are different in each region, we set Lamé constants $\mu = \mu^s$, $\lambda = \lambda^s$ on Ω^s for $s = +, -$.

Multiplying $\mathbf{v} \in (H_0^1(\Omega))^2$ and applying Green's identity in each domain Ω^s, we obtain

$$
\begin{aligned}
\int_{\Omega^s} 2\mu^s\boldsymbol{\epsilon}(\mathbf{u}) : \boldsymbol{\epsilon}(\mathbf{v})\,dx &+ \int_{\Omega^s} \lambda^s \operatorname{div}\mathbf{u}\operatorname{div}\mathbf{v}\,dx \\
&- \int_{\partial\Omega^s} \boldsymbol{\sigma}(\mathbf{u})\,\mathbf{n} \cdot \mathbf{v}\,ds = \int_{\Omega^s} \mathbf{f} \cdot \mathbf{v}\,dx,
\end{aligned}
\tag{8}
$$

where

$$\boldsymbol{\epsilon}(\mathbf{u}) : \boldsymbol{\epsilon}(\mathbf{v}) = \sum_{i,j=1}^{2} \epsilon_{ij}(\mathbf{u})\,\epsilon_{ij}(\mathbf{v}). \tag{9}$$

Summing over $s = +, -$ and applying the interior traction condition (4), we obtain the following weak form:

$$a(\mathbf{u}, \mathbf{v}) = (\mathbf{f}, \mathbf{v}), \tag{10}$$

where

$$a(\mathbf{u}, \mathbf{v}) = \int_\Omega 2\mu\boldsymbol{\epsilon}(\mathbf{u}) : \boldsymbol{\epsilon}(\mathbf{v})\,dx + \int_\Omega \lambda \operatorname{div}\mathbf{u}\operatorname{div}\mathbf{v}\,dx. \tag{11}$$

As usual, $(\cdot, \cdot)$ denotes the $L^2(\Omega)$ inner product. Then we have the following result [5, 13].

Theorem 1. *There exists a unique solution $\mathbf{u} \in (H_0^1(\Omega))^2$ of (2)–(5) satisfying and $\mathbf{u} \in (H^2(\Omega^s))^2$, $s = +, -$. Here, $H^1(\Omega), H^2(\Omega^s)$, and so forth are usual Sobolev spaces on respective domains and $H_0^1(\Omega)$ is a subspace of $H^1(\Omega)$ functions having zero trace.*

3. A Consistent IFEM Based on Crouzeix-Raviart (CR) Element

In this section, we propose a new IFEM for elasticity equation with interface, by modifying the method suggested in [10].

More specifically, we use the modified CR element [16] and add consistency terms similar to those of the discontinuous Galerkin (DG) formulation [17], but our methods have the same degrees of freedom as those in [10], which has the same degrees of freedom as the standard CR FEM. Here we need to clarify some notations. The bracket [·] means the jump across the interface:

$$[\mathbf{u}]_\Gamma := \mathbf{u}|_{\Omega^+} - \mathbf{u}|_{\Omega^-} . \tag{12}$$

Let $\{\mathscr{T}_h\}$ be a given quasi-uniform triangulations of Ω by the triangles of maximum diameter h. We allow the grid to be cut by the interface. Let the collection of all the interior edges of $T \in \mathscr{T}_h$ be denoted by $\mathscr{E}$. For every $e \in \mathscr{E}$, there are two elements T_1 and T_2 sharing e as a common edge. Let $\mathbf{n}_{T_i}, i = 1, 2$ be the unit outward normal vector to the boundary of T_i. We choose a direction of the normal vector, say $\mathbf{n}_e = \mathbf{n}_{T_1}$ for each edge e, and fix it once and for all. For functions v defined on $T_1 \cup T_2$, we let $\{\cdot\}$ denote the average across e; that is,

$$\{v\}_e = \frac{1}{2}\left(v|_{T_1} + v|_{T_2}\right). \tag{13}$$

We call an element $T \in \mathscr{T}_h$ an *interface element* if the interface Γ passes through the interior of T; otherwise, we call it a *noninterface* element. Let $\mathscr{T}_h^*$ be the collection of all interface elements. We assume the following situations which are easily satisfied when h is small enough:

  (i) The interface intersects the edges of an element at no more than two points.

  (ii) The interface intersects each edge at most once, except possibly it passes through two vertices.

The main idea of the IFEM for elasticity problem is to use two pieces of linear shape functions (vector form) on an interface element to construct a new shape function that satisfy the Laplace-Young condition. We set, for $i = 1, 2, \ldots, 6$,

$$\widehat{\boldsymbol{\phi}}_i(x, y)$$

$$= \begin{cases} \widehat{\boldsymbol{\phi}}_i^+(x, y) = \begin{pmatrix} \widehat{\phi}_{i1}^+ \\ \widehat{\phi}_{i2}^+ \end{pmatrix} = \begin{pmatrix} a_1^+ + b_1^+ x + c_1^+ y \\ a_2^+ + b_2^+ x + c_2^+ y \end{pmatrix}, & (x, y) \in T^+, \\ \widehat{\boldsymbol{\phi}}_i^-(x, y) = \begin{pmatrix} \widehat{\phi}_{i1}^- \\ \widehat{\phi}_{i2}^- \end{pmatrix} = \begin{pmatrix} a_1^- + b_1^- x + c_1^- y \\ a_2^- + b_2^- x + c_2^- y \end{pmatrix}, & (x, y) \in T^- \end{cases} \tag{14}$$

and require these functions that satisfy the nodal value conditions (edge average), continuity, and jump conditions along the interface (see Figure 2):

$$\overline{\widehat{\phi}_{i1}} \mid e_j = \delta_{ij}, \quad j = 1, 2, 3,$$

$$\overline{\widehat{\phi}_{i2}} \mid e_j = \delta_{(i-3)j}, \quad j = 1, 2, 3,$$

$$\left[\widehat{\boldsymbol{\phi}}_i(D)\right] = 0, \tag{15}$$

$$\left[\widehat{\boldsymbol{\phi}}_i(E)\right] = 0,$$

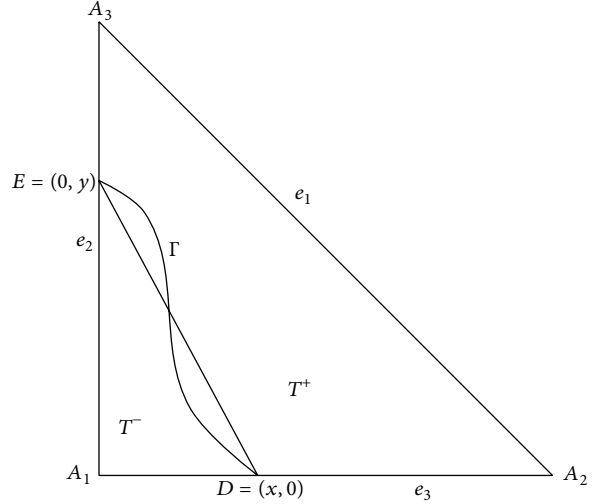$$\left[\boldsymbol{\sigma}\left(\widehat{\boldsymbol{\phi}}_i\right) \cdot \mathbf{n}\right]_{\overline{DE}} = 0.$$

Figure 2: A typical interface triangle.

It is shown in [10] that these twelve conditions uniquely determine the basis functions $\widehat{\boldsymbol{\phi}}_i, i = 1, \ldots, 6$.

We denote by $\widehat{\mathbf{N}}_h(T)$ the space of functions generated by $\widehat{\boldsymbol{\phi}}_i, i = 1, \ldots, 6$ constructed above. Using this local finite element space, we define the global *immersed finite element space* $\widehat{\mathbf{N}}_h(\Omega)$ by

$$\widehat{\mathbf{N}}_h(\Omega)$$

$$= \begin{cases} \widehat{\boldsymbol{\phi}} \in \widehat{\mathbf{N}}_h(T) & \text{if } T \in \mathscr{T}_h^*, \\ \widehat{\boldsymbol{\phi}} \in \mathbf{N}_h(T) & \text{if } T \notin \mathscr{T}_h^*; \\ \displaystyle\int_e \widehat{\boldsymbol{\phi}}\big|_{\partial T_1} ds = \int_e \widehat{\boldsymbol{\phi}}\big|_{\partial T_2} ds; & \text{if } T_1 \text{ and } T_2 \text{ share an edge } e \\ \displaystyle\int_{\partial T \cap \partial \Omega} \widehat{\boldsymbol{\phi}} \, ds = \mathbf{0}. \end{cases} \tag{16}$$

First we note the identity

$$ab - cd = \frac{1}{2}\left\{(a + c)(b - d) + (a - c)(b + d)\right\}. \tag{17}$$

Multiplying (2) by $\mathbf{v} \in (H^1(T))^2$, integration by parts and using (17), we see

$$\sum_{T \in \mathscr{T}_h} \left(\int_T 2\mu\boldsymbol{\epsilon}(\mathbf{u}) : \boldsymbol{\epsilon}(\mathbf{v}) \, dx + \int_T \lambda \operatorname{div} \mathbf{u} \operatorname{div} \mathbf{v} \, dx\right)$$

$$- \sum_{e \in \mathscr{E}} \int_e \{\boldsymbol{\sigma}(\mathbf{u}) \cdot \mathbf{n}_e\}_e [\mathbf{v}]_e \, ds = \int_\Omega \mathbf{f} \cdot \mathbf{v} \, dx. \tag{18}$$

We now propose an IFEM scheme for (2)–(5) based on the form (18).

CRIFEM-C. Find $\mathbf{u}_h \in \widehat{\mathbf{N}}_h(\Omega)$ such that

$$a_h(\mathbf{u}_h, \mathbf{v}_h) = (\mathbf{f}, \mathbf{v}_h), \quad \forall \mathbf{v}_h \in \widehat{\mathbf{N}}_h(\Omega), \tag{19}$$

where

$$a_h(\mathbf{u}, \mathbf{v}) := \sum_{T \in \mathcal{T}_h} \left(\int_T 2\mu \boldsymbol{\epsilon}(\mathbf{u}) : \boldsymbol{\epsilon}(\mathbf{v}) \, dx \right. \tag{20}$$

$$\left. + \int_T \lambda \operatorname{div} \mathbf{u} \operatorname{div} \mathbf{v} \, dx \right) + \sum_{e \in \mathcal{E}} \int_e \frac{\tau}{h} [\mathbf{u}][\mathbf{v}] \, ds$$

$$- \sum_{e \in \mathcal{E}} \int_e \{\boldsymbol{\sigma}(\mathbf{u}) \cdot \mathbf{n}\} \cdot [\mathbf{v}] \, ds - \epsilon \sum_{e \in \mathcal{E}} \int_e \{\boldsymbol{\sigma}(\mathbf{v}) \cdot \mathbf{n}\} \cdot [\mathbf{u}] \, ds, \tag{21}$$

$$\forall \mathbf{u}, \mathbf{v} \in \mathbf{H}_h(\Omega).$$

The variations of CRIFEM-C scheme are motivated to IIPG, SIPG, and NIPG of DG methods ($\epsilon = 0$, $\epsilon = 1$, and $\epsilon = -1$, resp.). In this paper we prove the case $\epsilon = 1$ only. Other cases can be similarly proved.

If the last two terms in (21) are not present, it is the same as the CRIFEM studied in [10]. The difference between our new scheme and CRIFEM lies in the consistency terms.

4. Error Analysis

We introduce necessary function spaces and norms. Let $m \geq 0$ be an integer. For any domain D, we let $H^m(D)$ be the usual Sobolev space with (semi)norms denoted by $|\cdot|_{m,D}$ and $\|\cdot\|_{m,D}$. For $m = 1, 2$ and any domain $D = T$ ($\in \mathcal{T}_h$) or $D = \Omega$, let

$$\left(\widetilde{H}^m(D)\right)^2 := \left\{ \mathbf{u} = (u_1, u_2) \in \left(H^{m-1}(D)\right)^2 : u|_{D \cap \Omega^s} \right. \tag{22}$$

$$\left. \in \left(H^m\left(D \cap \Omega^s\right)\right)^2, \ s = +, - \right\}$$

with norms

$$|\mathbf{u}|^2_{\widetilde{H}^m(D)} := |\mathbf{u}|^2_{m, D \cap \Omega^+} + |\mathbf{u}|^2_{m, D \cap \Omega^-},$$

$$\|\mathbf{u}\|^2_{\widetilde{H}^m(D)} := \|\mathbf{u}\|^2_{m-1, D} + |\mathbf{u}|^2_{\widetilde{H}^m(D)}. \tag{23}$$

When a finite element triangulation $\{\mathcal{T}_h\}$ is involved, the norm $\|\mathbf{u}\|^2_{\widetilde{H}^m(D)}$ is understood as piecewise: $\left(\sum_{T \in \mathcal{T}_h} \|\mathbf{u}\|^2_{\widetilde{H}^m(T)}\right)^{1/2}$ and denote it by $\|\mathbf{u}\|_{m,h}$. Let $\mathbf{H}_h(\Omega) := (H_0^1(\Omega))^2 + \widehat{\mathbf{N}}_h(\Omega)$. We need subspaces of $(\widetilde{H}^2(T))^2$ and $(\widetilde{H}^2(\Omega))^2$ satisfying the jump conditions:

$$\left(\widetilde{H}^2_\Gamma(T)\right)^2 := \left\{ \mathbf{u} \in \left(\widetilde{H}^2(T)\right)^2, \ [\boldsymbol{\sigma}(\mathbf{u}) \cdot \mathbf{n}]_{\Gamma \cap T} = 0 \right\},$$

$$\left(\widetilde{H}^2_\Gamma(\Omega)\right)^2 \tag{24}$$

$$:= \left\{ \mathbf{u} \in \left(H_0^1(\Omega)\right)^2, \ \mathbf{u}|_T \in \left(\widetilde{H}^2_\Gamma(T)\right)^2, \ \forall T \in \mathcal{T}_h \right\}.$$

At last, we introduce the following mesh dependent energy-like norms

$$\|\mathbf{v}\|^2_{a_h} := \sum_{T \in \mathcal{T}_h} \|\mathbf{v}\|^2_{a,T} \tag{25}$$

$$+ \sum_{e \in \mathcal{E}} \left(\int_e h |\{\boldsymbol{\sigma}(\mathbf{v}) \cdot \mathbf{n}\}|^2 \, ds + \int_e \frac{\tau}{h} [\mathbf{v}]^2 \, ds \right),$$

where

$$\|\mathbf{v}\|^2_{a,T} = \int_T 2\mu \boldsymbol{\epsilon}(\mathbf{v}) : \boldsymbol{\epsilon}(\mathbf{v}) \, dx + \int_T \lambda |\operatorname{div} \mathbf{v}|^2 \, dx. \tag{26}$$

Throughout the paper, the constants C, C_0, C_1, and so forth are generic constants independent of the mesh size h and functions $\mathbf{u}, \mathbf{v}$ but may depend on the problem data $\mu, \lambda, \mathbf{f}$, and Ω and are not necessarily the same on each occurrence.

4.1. Approximation Property of $\widehat{\mathbf{N}}_h(T)$. We need an interpolation operator: for any $\mathbf{u} \in (H^1(T))^2$, we define $I_h \mathbf{u} \in \widehat{\mathbf{N}}_h(T)$ using the average of $\mathbf{u}$ on each edge of T by

$$\int_{e_i} I_h \mathbf{u} \, ds = \int_{e_i} \mathbf{u} \, ds, \quad i = 1, 2, 3 \tag{27}$$

and call $I_h \mathbf{u}$ the *interpolant* of $\mathbf{u}$ in $\widehat{\mathbf{N}}_h(T)$. We then define $I_h \mathbf{u}$ for $\mathbf{u} \in (H^1(\Omega))^2$ by $(I_h \mathbf{u})|_T = I_h(\mathbf{u}|_T)$. The following result is shown in [10].

Proposition 2. *For any $\mathbf{u} \in (\widetilde{H}^2_\Gamma(\Omega))^2$, there exists a constant $C > 0$ such that for $m = 0, 1$*

$$\|\mathbf{u} - I_h \mathbf{u}\|_{m,h} + m \cdot \left\| \sqrt{\lambda} \operatorname{div}(\mathbf{u} - I_h \mathbf{u}) \right\|_{L^2(\Omega)}$$

$$\leq C h^{2-m} \left(\|\mathbf{u}\|_{\widetilde{H}^2(\Omega)} + m \cdot \sqrt{\lambda_M} \|\operatorname{div} \mathbf{u}\|_{\widetilde{H}^1(\Omega)} \right), \tag{28}$$

$$\|\mathbf{u} - I_h \mathbf{u}\|_{m,h} \leq C h^{2-m} \|\mathbf{u}\|_{\widetilde{H}^2(\Omega)},$$

where $\lambda_M := \max_{s=+,-} \lambda^s$.

Proposition 3. *Let $\mathbf{u}$ be the solution of (2). We have*

$$\|\mathbf{u} - I_h \mathbf{u}\|_{a_h} \leq C h \left(\|\mathbf{u}\|_{\widetilde{H}^2(\Omega)} + \sqrt{\lambda_M} \|\operatorname{div} \mathbf{u}\|_{\widetilde{H}^1(\Omega)} \right), \tag{29}$$

for some constant $C > 0$.

Proof. Since the estimates of other terms are given in [10], it suffices to show that the term $\sum_{e \in \mathcal{E}} \int_e h |\{\boldsymbol{\sigma}(\mathbf{u} - I_h \mathbf{u}) \cdot \mathbf{n}\}|^2 ds$ is bounded by $\|\mathbf{u} - I_h \mathbf{u}\|_{1,h}$. It can be proved by splitting $\boldsymbol{\sigma}(\mathbf{u} - I_h \mathbf{u}) \cdot \mathbf{n}$ into normal and tangential component; see [18] for details. The conclusion will follow from Proposition 2. □

To prove the coercivity of our bilinear form, we need the following lemmas.

Lemma 4 (Korn's inequality [5, 19]). *Let $D \subset \mathbb{R}^n$, $n = 2, 3$ be a simply connected domain. There exists constant $C(D) > 0$ such that*

$$|\mathbf{v}|^2_{H^1(D)} \leq C \left(\|\boldsymbol{\epsilon}(\mathbf{v})\|^2_{L^2(D)} + \|Q(\mathbf{v})\|^2_{L^2(D)} \right), \tag{30}$$

$$\forall \mathbf{v} \in \left(H^1(D)\right)^n,$$

where $Q(\mathbf{v}) := \mathbf{v} - (1/|D|) \int_D \mathbf{v} \, dx$.

Corollary 5. *There exists constant $\widehat{C}_0 > 0$ such that*

$$|\mathbf{v}_h|_{1,T} \leq \widehat{C}_0 \|\mathbf{v}_h\|_{a,T}, \quad \forall \mathbf{v}_h \in \widehat{\mathbf{N}}(T). \tag{31}$$

Proof. By Lemma 4 and approximation property, we have

$$
\begin{aligned}
|\mathbf{v}_h|_{1,T}^2 &\leq C \left(\|\boldsymbol{\epsilon}(\mathbf{v}_h)\|_{L^2(T)}^2 + \|Q(\mathbf{v}_h)\|_{L^2(T)}^2 \right) \\
&\leq C \left(\|\mathbf{v}_h\|_{a,T}^2 + Ch \, |\mathbf{v}_h|_{1,T}^2 \right).
\end{aligned}
\tag{32}
$$

Hence, we get the result. $\qquad\square$

Lemma 6. *There exists constant $\widehat{C}_1 > 0$ such that*

$$h \|\boldsymbol{\sigma}(\mathbf{v}_h) \cdot \mathbf{n}\|_{0,e}^2 \leq \widehat{C}_1 \|\nabla \mathbf{v}_h\|_{0,T}^2, \quad \forall \mathbf{v}_h \in \widehat{\mathbf{N}}(T), \tag{33}$$

where $e \subset \partial T$ is an edge of T.

Proof. It can be obtained by the similar technique in [18]. $\quad\square$

Now we show a_h-form is bounded and coercive.

Lemma 7. *If we choose τ large enough, there exists constant $C_0, C_1 > 0$ such that the following holds:*

$$
\begin{aligned}
a_h(\mathbf{u}, \mathbf{v}) &\leq C_0 \|\mathbf{u}\|_{a_h} \|\mathbf{v}\|_{a_h}, \quad \forall \mathbf{u}, \mathbf{v} \in \mathbf{H}_h, \\
C_1 \|\mathbf{v}_h\|_{a_h}^2 &\leq a_h(\mathbf{v}_h, \mathbf{v}_h), \quad \forall \mathbf{v}_h \in \widehat{\mathbf{N}}_h.
\end{aligned}
\tag{34}
$$

Proof. Boundedness is trivial by definition of a_h-form. Using Corollary 5 and using Lemma 6 we have

$$
\begin{aligned}
&\sum_{e \in \mathscr{E}} \int_e \{\boldsymbol{\sigma}(\mathbf{v}_h) \cdot \mathbf{n}\} [\mathbf{v}_h] \, ds \\
&\leq \left(\sum_{e \in \mathscr{E}} h \|\{\boldsymbol{\sigma}(\mathbf{v}_h) \mathbf{n}\}\|_{0,e}^2 \right)^{1/2} \left(\sum_{e \in \mathscr{E}} h^{-1} \|[\mathbf{v}_h]\|_{0,e}^2 \right)^{1/2} \\
&\leq \left(\widehat{C}_1 \sum_{T \in \mathscr{T}_h} \|\nabla \mathbf{v}_h\|_{0,T}^2 \right)^{1/2} \left(\sum_{e \in \mathscr{E}} h^{-1} \|[\mathbf{v}_h]\|_{0,e}^2 \right)^{1/2} \\
&\leq \left(\widehat{C}_0 \widehat{C}_1 \sum_{T \in \mathscr{T}_h} \|\mathbf{v}_h\|_{a,T}^2 \right)^{1/2} \left(\sum_{e \in \mathscr{E}} h^{-1} \|[\mathbf{v}_h]\|_{0,e}^2 \right)^{1/2} \\
&\leq \frac{\gamma}{2} \left(\sum_{T \in \mathscr{T}_h} \|\mathbf{v}_h\|_{a,T}^2 \right) + \frac{\widehat{C}_0 \widehat{C}_1}{2\gamma} \left(\sum_{e \in \mathscr{E}} h^{-1} \|[\mathbf{v}_h]\|_{0,e}^2 \right)
\end{aligned}
\tag{35}
$$

for every $\gamma > 0$. Hence, we have

$$
\begin{aligned}
a_h(\mathbf{v}_h, \mathbf{v}_h) &= \sum_{T \in \mathscr{T}_h} \|\mathbf{v}_h\|_{a,T}^2 + \sum_{e \in \mathscr{E}} \int_e \frac{\tau}{h} [\mathbf{v}_h]^2 \, ds \\
&\quad - 2 \sum_{e \in \mathscr{E}} \int_e \{\boldsymbol{\sigma}(\mathbf{v}_h) \cdot \mathbf{n}\} [\mathbf{v}_h] \, ds \\
&\geq (1 - \gamma) \sum_{T \in \mathscr{T}_h} \|\mathbf{v}_h\|_{a,T}^2 \\
&\quad + \left(\frac{\tau}{h} - \frac{\widehat{C}_0 \widehat{C}_1}{h\gamma} \right) \sum_{e \in \mathscr{E}} \int_e [\mathbf{v}_h]^2 \, ds \\
&\geq \frac{1 - \gamma}{1 + \widehat{C}_1} \sum_{T \in \mathscr{T}_h} \|\mathbf{v}_h\|_{a,T}^2 \\
&\quad + \frac{\tau}{h} \left(1 - \frac{\widehat{C}_0 \widehat{C}_1}{\tau \gamma} \right) \sum_{e \in \mathscr{E}} \int_e [\mathbf{v}_h]^2 \, ds \\
&\quad + \frac{(1 - \gamma) \widehat{C}_1}{(1 + \widehat{C}_1)} \sum_{T \in \mathscr{T}_h} \|\mathbf{v}_h\|_{a,T}^2 \\
&\geq \frac{1 - \gamma}{1 + \widehat{C}_1} \sum_{T \in \mathscr{T}_h} \|\mathbf{v}_h\|_{a,T}^2 \\
&\quad + \frac{\tau}{h} \left(1 - \frac{\widehat{C}_0 \widehat{C}_1}{\tau \gamma} \right) \sum_{e \in \mathscr{E}} \int_e [\mathbf{v}_h]^2 \, ds \\
&\quad + \frac{(1 - \gamma)}{(1 + \widehat{C}_1) \widehat{C}_0} \sum_{e \in \mathscr{E}} \int_e h \, |\{\boldsymbol{\sigma}(\mathbf{v}_h) \cdot \mathbf{n}\}|^2 \, ds
\end{aligned}
\tag{36}
$$

since

$$
\begin{aligned}
\sum_{e \in \mathscr{E}} \int_e h \, |\{\boldsymbol{\sigma}(\mathbf{v}_h) \cdot \mathbf{n}\}|^2 \, ds &\leq \widehat{C}_1 \sum_{T \in \mathscr{T}_h} \|\nabla \mathbf{v}_h\|_{0,T}^2 \\
&\leq \widehat{C}_0 \widehat{C}_1 \sum_{T \in \mathscr{T}_h} \|\mathbf{v}_h\|_{a,T}^2 .
\end{aligned}
\tag{37}
$$

If we choose $\gamma < 1$ and τ large enough so that $(1 - \widehat{C}_0 \widehat{C}_1 / \tau \gamma) > 0$, then with $C_c := \min((1 - \gamma)/(1 + \widehat{C}_1), 1 - \widehat{C}_0 \widehat{C}_1 / \tau \gamma, (1 - \gamma)/(1 + \widehat{C}_1) \widehat{C}_0)$, we have

$$a_h(\mathbf{v}_h, \mathbf{v}_h) \geq C_c \|\mathbf{v}_h\|_{a_h}^2 . \tag{38}$$

$\square$

Now we are ready to show our main result.

Theorem 8. *Let $\mathbf{u}$ (resp., $\mathbf{u}_h$) be the solution of (2) (resp., (19)). Then we have*

$$\|\mathbf{u} - \mathbf{u}_h\|_{a_h} \leq Ch \left(\|\mathbf{u}\|_{\widetilde{H}^2(\Omega)} + \sqrt{\lambda_M} \|\mathrm{div}\, \mathbf{u}\|_{\widetilde{H}^1(\Omega)} \right). \tag{39}$$

Proof. By triangular inequality, we have

$$\|\mathbf{u} - \mathbf{u}_h\|_{a_h} \leq \|\mathbf{u}_h - I_h \mathbf{u}\|_{a_h} + \|\mathbf{u} - I_h \mathbf{u}\|_{a_h} . \tag{40}$$

From Lemma 7, it follows that

$$c \left\| \mathbf{u}_h - I_h \mathbf{u} \right\|_{a_h}^2 \leq a_h \left(\mathbf{u}_h - I_h \mathbf{u}, \mathbf{u}_h - I_h \mathbf{u} \right)$$

$$= a_h \left(\mathbf{u} - I_h \mathbf{u}, \mathbf{u}_h - I_h \mathbf{u} \right) \quad (41)$$

$$\leq C_0 \left\| \mathbf{u}_h - I_h \mathbf{u} \right\|_{a_h} \left\| \mathbf{u} - I_h \mathbf{u} \right\|_{a_h}.$$

So we have

$$\left\| \mathbf{u}_h - I_h \mathbf{u} \right\|_{a_h} \leq C \left\| \mathbf{u} - I_h \mathbf{u} \right\|_{a_h}. \quad (42)$$

By Proposition 3, we have

$$\left\| \mathbf{u} - \mathbf{u}_h \right\|_{a_h} \leq C \left\| \mathbf{u} - I_h \mathbf{u} \right\|_{a_h}$$

$$\leq Ch \left(\left\| \mathbf{u} \right\|_{\widetilde{H}^2(\Omega)} + \sqrt{\lambda_M} \left\| \mathrm{div}\, \mathbf{u} \right\|_{\widetilde{H}^1(\Omega)} \right). \quad (43)$$

□

Remark 9. If, in addition, the following relation

$$2\mu \left\| \mathbf{u} \right\|_{\widetilde{H}^2(\Omega)} + \lambda \left\| \mathrm{div}\, \mathbf{u} \right\|_{\widetilde{H}^1(\Omega)} \leq C \left\| \mathbf{f} \right\|_{L^2(\Omega)} \quad (44)$$

holds, then the result of Theorem 8 becomes

$$\left\| \mathbf{u} - \mathbf{u}_h \right\|_{a_h} \leq Ch \left\| \mathbf{f} \right\|_{L^2(\Omega)}. \quad (45)$$

It means that the our estimate holds uniformly when $\lambda \to \infty$. Furthermore, one can show the following L^2 estimate by the standard duality argument:

$$\left\| \mathbf{u} - \mathbf{u}_h \right\|_{L^2(\Omega)} \leq Ch^2 \left\| \mathbf{f} \right\|_{L^2(\Omega)}. \quad (46)$$

5. Numerical Results

In this section we present numerical examples. The domain is $\Omega = (-1, 1) \times (-1, 1)$. The interface is the zero set of $L(x, y) = x^2 + y^2 - r_0^2$. Let $\Omega^+ = \Omega \cap \{(x, y) \mid L(x, y) > 0\}$, $\Omega^- = \Omega \cap \{(x, y) \mid L(x, y) < 0\}$. The exact solution is chosen as

$$\mathbf{u} = \left(\frac{1}{\mu} \left(x^2 + y^2 - r_0^2 \right) x, \frac{1}{\mu} \left(x^2 + y^2 - r_0^2 \right) y \right) \quad (47)$$

with various values of μ and λ. For numerical simulation we partition the domain into uniform right triangles having size $h = 2^{-k}, k = 3, 4, \ldots$.

Example 1. In this example, we test two sets of parameters and radii of the interface.

(1) We choose $\mu^- = 1$, $\mu^+ = 100$, $\lambda = 5\mu$, and $r_0 = 0.36$.

(2) We choose $\mu^- = 1$, $\mu^+ = 10$, $\lambda = 5\mu$, and $r_0 = 0.48$.

Tables 1 and 2 show the convergence behavior of our numerical schemes for both examples. In both cases, we see the optimal order of convergence in L^2, H^1, and divergence norms. x-components of the solution are plotted in Figures 3 and 4.
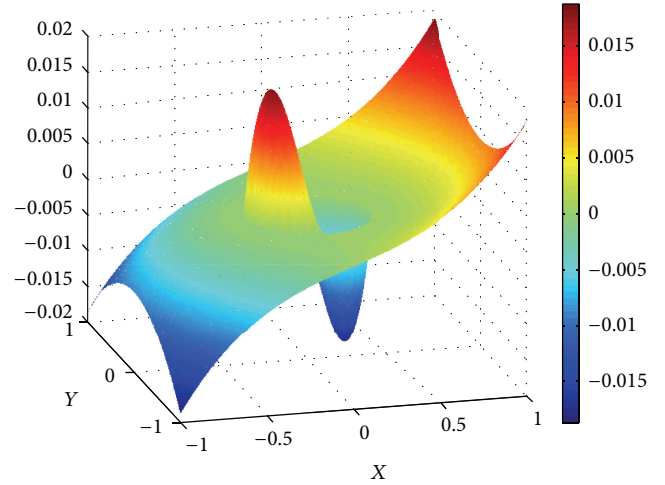

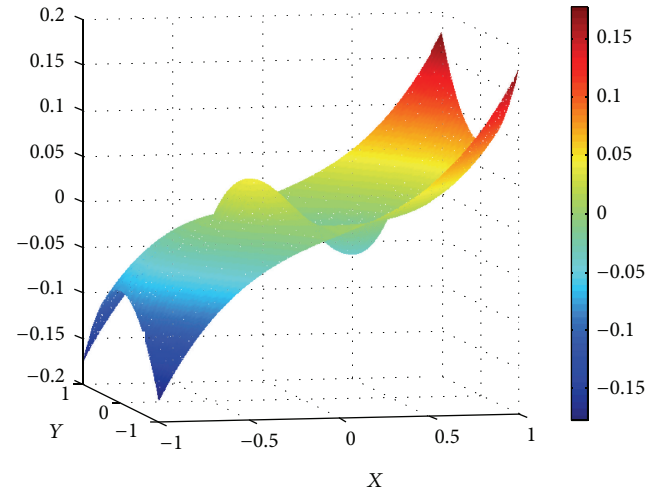FIGURE 3: x-component, $\mu^- = 1$, $\mu^+ = 100$, $\lambda = 5\mu$.

FIGURE 4: x-component, $\mu^- = 1$, $\mu^+ = 10$, $\lambda = 5\mu$.

Example 2 (nearly incompressible case). (1) We let $\mu^- = 1$, $\mu^+ = 10$, $\lambda = 100\mu$, $\nu = 0.495$, and $r_0 = 0.7$.

(2) We let $\mu^- = 1$, $\mu^+ = 10$, $\lambda = 1000\mu$, $\nu = 0.4995$, and $r_0 = 0.6$.

Tables 3 and 4 show the convergence behavior. In both cases, we see the optimal order of convergence in L^2, H^1, and divergence norms. No locking phenomena occurs in both cases. Again x-components of the solution are plotted in Figures 5 and 6.

Example 3 (ellipse interface case). Next we consider examples with elliptic shaped interface. The domain is the same as above, and the interface is represented by $L(x, y) = x^2/4 + y^2 - r_0^2 = 0$. The exact solution is chosen as

$$\mathbf{u} = \left(\frac{1}{\mu} \left(\frac{x^2}{4} + y^2 - r_0^2 \right) x, \frac{1}{\mu} \left(\frac{x^2}{4} + y^2 - r_0^2 \right) y \right) \quad (48)$$

with various values of μ and λ.

TABLE 1: $\mu^- = 1$, $\mu^+ = 100$, and $\lambda = 5\mu$.

$1/h$	$\|\mathbf{u} - \mathbf{u}_h\|_0$	Order	$\|\mathbf{u} - \mathbf{u}_h\|_{1,h}$	Order	$\|\text{div } \mathbf{u} - \text{div } \mathbf{u}_h\|_0$	Order
8	$1.271e-3$		$4.230e-2$		$3.950e-2$	
16	$3.096e-4$	2.038	$1.979e-2$	1.119	$1.834e-2$	1.107
32	$6.461e-5$	2.261	$9.780e-3$	1.017	$9.374e-3$	0.968
64	$1.534e-5$	2.075	$4.899e-3$	0.977	$4.790e-3$	0.969
128	$3.636e-6$	2.076	$2.432e-3$	1.011	$2.412e-3$	0.990
256	$8.882e-7$	2.033	$1.214e-3$	1.003	$1.210e-3$	0.995

TABLE 2: $\mu^- = 1$, $\mu^+ = 10$, and $\lambda = 5\mu$.

$1/h$	$\|\mathbf{u} - \mathbf{u}_h\|_0$	Order	$\|\mathbf{u} - \mathbf{u}_h\|_{1,h}$	Order	$\|\text{div } \mathbf{u} - \text{div } \mathbf{u}_h\|_0$	Order
8	$1.729e-3$		$7.374e-2$		$7.260e-2$	
16	$4.147e-4$	2.060	$3.786e-2$	0.962	$3.774e-2$	0.944
32	$1.030e-4$	2.009	$1.938e-2$	0.966	$1.934e-2$	0.965
64	$2.565e-5$	2.007	$9.734e-3$	0.993	$9.744e-3$	0.989
128	$6.384e-6$	2.006	$4.886e-3$	0.994	$4.897e-3$	0.993
256	$1.590e-6$	2.005	$2.447e-3$	0.998	$2.454e-3$	0.997

TABLE 3: $\mu^- = 1$, $\mu^+ = 10$, and $\lambda = 100\mu$.

$1/h$	$\|\mathbf{u} - \mathbf{u}_h\|_0$	Order	$\|\mathbf{u} - \mathbf{u}_h\|_{1,h}$	Order	$\|\text{div } \mathbf{u} - \text{div } \mathbf{u}_h\|_0$	Order
8	$7.748e-3$		$2.156e-1$		$1.457e-1$	
16	$2.432e-3$	1.672	$1.126e-1$	0.937	$7.363e-2$	0.985
32	$7.363e-4$	1.724	$5.533e-2$	1.025	$3.724e-2$	0.983
64	$2.121e-4$	1.796	$2.735e-2$	1.016	$1.876e-2$	0.989
128	$5.475e-5$	1.954	$1.349e-2$	1.020	$9.417e-3$	0.994
256	$1.409e-5$	1.959	$6.689e-3$	1.012	$4.719e-3$	0.997

TABLE 4: $\mu^- = 1$, $\mu^+ = 10$, and $\lambda = 1000\mu$.

$1/h$	$\|\mathbf{u} - \mathbf{u}_h\|_0$	Order	$\|\mathbf{u} - \mathbf{u}_h\|_{1,h}$	Order	$\|\text{div } \mathbf{u} - \text{div } \mathbf{u}_h\|_0$	Order
8	$7.799e-2$		$1.636e-0$		$1.059e-1$	
16	$2.418e-2$	1.689	$9.117e-1$	0.844	$5.514e-2$	0.942
32	$6.848e-2$	1.820	$4.521e-1$	1.012	$2.817e-2$	0.969
64	$1.860e-3$	1.880	$2.249e-1$	1.007	$1.417e-2$	0.991
128	$4.848e-4$	1.940	$1.112e-1$	1.016	$7.110e-3$	0.995
256	$1.237e-4$	1.971	$5.536e-2$	1.006	$3.563e-3$	0.997

(1) We let $\mu^- = 1$, $\mu^+ = 10$, $\lambda = 5\mu$, $r_0 = 0.4$.

(2) We let $\mu^- = 1$, $\mu^+ = 100$, $\lambda = 5\mu$, $r_0 = 0.3$.

Tables 5 and 6 show the convergence behavior. We observe similar optimal convergence rates for all norms. Figures 7 and 8 show the x-components of the solution.

Example 4 (unknown solution). This last example computes a problem with unknown solution. We choose $\mu^- = 1$, $\mu^+ = 100$, $\nu^- = 0.28$, $\nu^+ = 0.4$, $r_0 = 0.3$, and $\mathbf{F} = (-11/4 -$ $(\lambda/\mu)x, -29/4 - (\lambda/\mu)y)$ with the same elliptical interface as in the previous example.

Figure 9 shows the x-component of the computed solution.

6. Conclusion

We presented a numerical scheme using a uniform grid for the elasticity problem with an interface. This is a modification of the scheme studied in [10] by adding consistency terms.

TABLE 5: $\mu^- = 1$, $\mu^+ = 10$, $\lambda = 5\mu$, and elliptical interface.

$1/h$	$\|\mathbf{u} - \mathbf{u}_h\|_0$	Order	$\|\mathbf{u} - \mathbf{u}_h\|_{1,h}$	Order	$\|\text{div } \mathbf{u} - \text{div } \mathbf{u}_h\|_0$	Order
8	$1.791e - 3$		$6.431e - 2$		$5.906e - 2$	
16	$4.543e - 4$	1.979	$3.105e - 2$	1.050	$2.902e - 2$	1.025
32	$1.139e - 4$	1.996	$1.568e - 2$	0.986	$1.474e - 2$	0.977
64	$2.785e - 5$	2.032	$7.908e - 3$	0.987	$7.452e - 3$	0.984
128	$6.969e - 6$	1.999	$3.970e - 3$	0.994	$3.747e - 3$	0.992
256	$1.740e - 6$	2.002	$1.988e - 3$	0.998	$1.878e - 3$	0.997

TABLE 6: $\mu^- = 1$, $\mu^+ = 100$, $\lambda = 5\mu$, and elliptical interface.

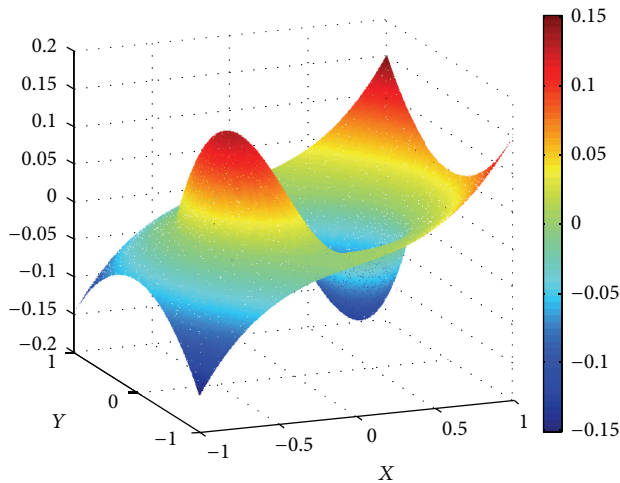| $1/h$	$\|\mathbf{u} - \mathbf{u}_h\|_0$	Order	$\|\mathbf{u} - \mathbf{u}_h\|_{1,h}$	Order	$\|\text{div } \mathbf{u} - \text{div } \mathbf{u}_h\|_0$	Order
8	$1.299e - 3$		$3.532e - 2$		$3.108e - 2$	
16	$4.055e - 4$	1.680	$1.681e - 2$	1.072	$1.389e - 2$	1.162
32	$8.503e - 5$	2.254	$8.272e - 3$	1.023	$7.251e - 3$	0.937
64	$1.848e - 5$	2.202	$4.089e - 3$	1.016	$3.713e - 3$	0.966
128	$4.517e - 6$	2.032	$2.041e - 3$	1.002	$1.869e - 3$	0.990
256	$1.116e - 6$	2.017	$1.020e - 3$	1.001	$9.385e - 4$	0.994

FIGURE 5: x-component, $\mu^- = 1$, $\mu^+ = 10$, $\lambda = 100\mu$.
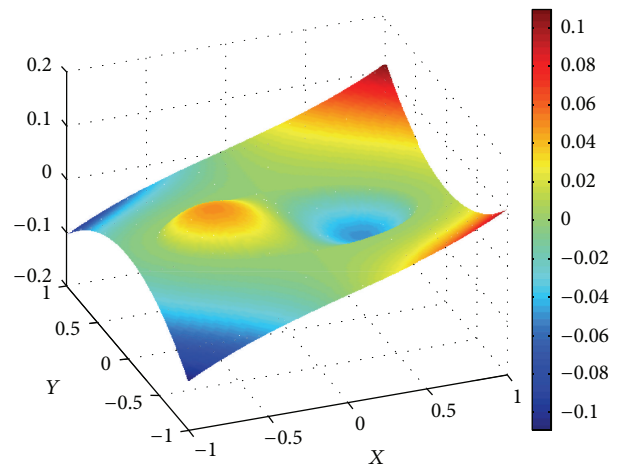

FIGURE 7: x-component, $\mu^- = 1$, $\mu^+ = 10$, $\lambda = 5\mu$ elliptical interface.
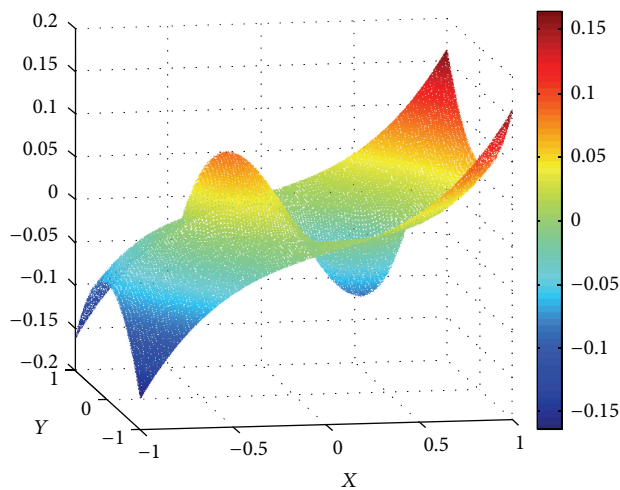

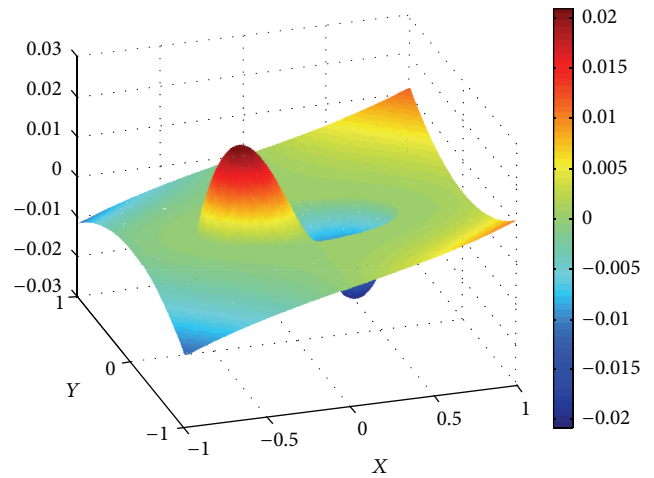FIGURE 6: x-component, $\mu^- = 1$, $\mu^+ = 10$, $\lambda = 1000\mu$.

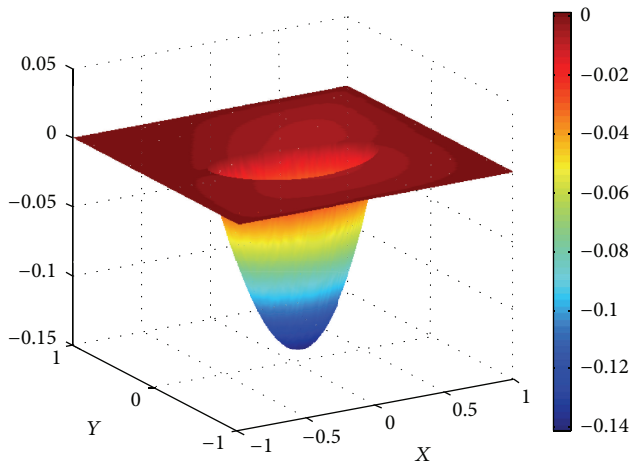FIGURE 8: x-component, $\mu^- = 1$, $\mu^+ = 100$, $\lambda = 5\mu$ elliptical interface.

FIGURE 9: x-component, $\mu^- = 1$, $\mu^+ = 100$, $\nu^- = 0.28$, $\nu^+ = 0.4$, $r_0 = 0.3$ unknown solution.

This scheme is very useful in computing problems with moving interface since we use a grid independent of the interface. We proved an optimal order of convergence in H^1-norm with minimal assumption. Numerical results show the efficiency of our method.
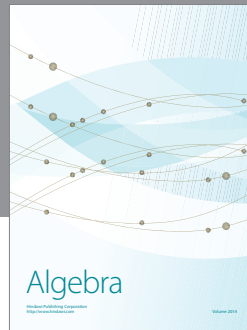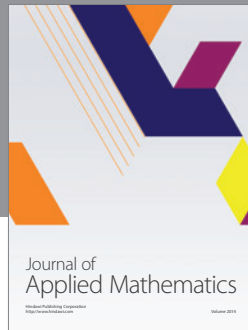
Competing Interests

The authors declare that they have no competing interests.

Acknowledgments

References

[1] V. Rutka and A. Wiegmann, "A fast finite difference method for elliptic PDEs in domains with non-grid aligned boundaries with application to 3D linear elasticity," in *Progress in Industrial Mathematics at ECMI 2002*, vol. 5, pp. 363–367, The European Consortium for Mathematics in Industry, 2004.

[2] P. Moin, *Engineering Numerical Analysis*, Cambridge University Press, Cambridge, UK, 2001.

[3] S. Yu, Y. Zhou, and G. W. Wei, "Matched interface and boundary (MIB) method for elliptic problems with sharp-edged interfaces," *Journal of Computational Physics*, vol. 224, no. 2, pp. 729–756, 2007.

[4] F. Chen and H. Chen, "A broken P_1-nonconforming finite element method for incompressible miscible displacement problem in porous media," *ISRN Applied Mathematics*, vol. 2013, Article ID 498383, 7 pages, 2013.

[5] P. G. Ciarlet, *Mathematical Elasticity, Volume I*, North-Holland Publishing, 1988.

[6] M. Oevermann, C. Scharfenberg, and R. Klein, "A sharp interface finite volume method for elliptic equations on Cartesian grids," *Journal of Computational Physics*, vol. 228, no. 14, pp. 5184–5206, 2009.

[7] S. C. Brenner and L.-Y. Sung, "Linear finite element methods for planar linear elasticity," *Mathematics of Computation*, vol. 59, no. 200, pp. 321–338, 1992.

[8] R. S. Falk, "Nonconforming finite element methods for the equations of linear elasticity," *Mathematics of Computation*, vol. 57, no. 196, pp. 529–550, 1991.

[9] T. Lin, D. Sheen, and X. Zhang, "A locking-free immersed finite element method for planar elasticity interface problems," *Journal of Computational Physics*, vol. 247, pp. 228–247, 2013.

[10] D. Y. Kwak, S. Jin, and D. Kyeong, "A stabilized P_1-nonconforming immersed finite element method for the interface elasticity problems," *ESAIM:M2AN*, 2016.

[11] D. Y. Kwak, K. T. Wee, and K. S. Chang, "An analysis of a broken P1-nonconforming finite element method for interface problems," *SIAM Journal on Numerical Analysis*, vol. 48, pp. 2117–2134, 2010.

[12] S. Hou and X.-D. Liu, "A numerical method for solving variable coefficient elliptic equation with interfaces," *Journal of Computational Physics*, vol. 202, no. 2, pp. 411–445, 2005.

[13] P. Hansbo and M. G. Larson, "Discontinuous Galerkin and the Crouzeix-Raviart element: applications to elasticity," *ESAIM: Mathematical Modelling and Numerical Analysis*, vol. 37, pp. 63–72, 2003.

[14] A. Hansbo and P. Hansbo, "A finite element method for the simulation of strong and weak discontinuities in solid mechanics," *Computer Methods in Applied Mechanics and Engineering*, vol. 193, no. 33-35, pp. 3523–3540, 2004.

[15] R. Becker, E. Burman, and P. Hansbo, "A Nitsche extended finite element method for incompressible elasticity with discontinuous modulus of elasticity," *Computer Methods in Applied Mechanics and Engineering*, vol. 198, no. 41–44, pp. 3352–3360, 2009.

[16] M. Crouzeix and P.-A. Raviart, "Conforming and nonconforming finite element methods for solving the stationary Stokes equations I," *ESAIM: Mathematical Modelling and Numerical Analysis—Modélisation Mathématique et Analyse Numérique*, vol. 7, no. 3, pp. 33–75, 1973.

[17] D. Arnold, F. Brezzi, B. Cockburn, and D. Marini, "Discontinuous Galerkin methods for elliptic problems," in *Discontinuous Galerkin Methods. Theory, Computation and Applications*, B. Cockburn, G. E. Karniadakis, and C.-W. Shu, Eds., vol. 11 of *Lecture Notes in Computational Science and Engineering*, pp. 89–101, Springer, New York, NY, USA, 2000.

[18] D. Y. Kwak and J. Lee, "A modified P1-immersed finite element method," *International Journal of Pure and Applied Mathematics*, vol. 104, no. 3, pp. 471–494, 2015.

[19] S. C. Brenner, "Korn's inequalities for piecewise H^1 vector fields," *Mathematics of Computation*, vol. 72, no. 247, pp. 1067–1087, 2003.